

A 1-D modelling of streaming potential dependence on water content during drainage experiment in sand

V. Allège,¹ F. Lehmann,² P. Ackerer,² L. Jouniaux¹ and P. Sailhac¹

¹Institut de Physique du Globe de Strasbourg, Uds/CNRS UMR-7516, Université de Strasbourg, 5 rue René Descartes, 67084, Strasbourg, France.

E-mail: vincent.allegre@unistra.fr

²Laboratoire d'Hydrologie et de Géochimie de Strasbourg, Uds/CNRS UMR-7517, Université de Strasbourg, 1 rue Blessig, 67000, Strasbourg, France

Accepted 2012 January 9. Received 2011 September 19; in original form 2011 March 22

SUMMARY

The understanding of electrokinetics for unsaturated conditions is crucial for numerous of geophysical data interpretation. Nevertheless, the behaviour of the streaming potential coefficient C as a function of the water saturation S_w is still discussed. We propose here to model both the Richards' equation for hydrodynamics and the Poisson's equation for electrical potential for unsaturated conditions using 1-D finite element method. The equations are first presented and the numerical scheme is then detailed for the Poisson's equation. Then, computed streaming potentials (SPs) are compared to recently published SP measurements carried out during drainage experiment in a sand column. We show that the apparent measurement of $\Delta V/\Delta P$ for the dipoles can provide the SP coefficient in these conditions. Two tests have been performed using existing models for the SP coefficient and a third one using a new relation. The results show that existing models of unsaturated SP coefficients $C(S_w)$ provide poor results in terms of SP magnitude and behaviour. We demonstrate that the unsaturated SP coefficient can be until one order of magnitude larger than C_{sat} , its value at saturation. We finally prove that the SP coefficient follows a non-monotonous behaviour with respect to water saturation.

Key words: Electrical properties; Electromagnetic theory; Hydrogeophysics; Hydrology; Permeability and porosity.

1 INTRODUCTION

Electric and electromagnetic methods are used in a large range of geophysical applications because of their sensitivity to fluids within the crust. The electrical resistivity can be related to the permeability and to the deformation, in full-saturated or in partially saturated conditions (Jouniaux *et al.* 1994, 2006; Henry *et al.* 2003; Doussan & Ruy 2009). The self-potentials have also been successfully used in the last decades. Self-potentials have been observed to detect contaminant plumes or salted fronts through the interpretation of electrochemical effects (Naudet *et al.* 2003; Maineult *et al.* 2006a,b). Most of the self-potential observations are interpreted through the electrokinetic effect. It has been proposed to use this electrokinetic effect for the seismic prediction For hydrological applications, some hydraulic properties can be inferred from the self-potential observations (Gibert & Pessel 2001; Sailhac *et al.* 2004; Glover *et al.* 2006; Glover & Walker 2009). The W -shaped anomalies classically observed on active volcanoes are used to characterize geothermal circulations (Finizola *et al.* 2002, 2004; Saracco *et al.* 2004; Onizawa *et al.* 2009; Mauri *et al.* 2010). It has also been proposed to use the self-potential monitoring to detect at distance the propagation

of a water front in a reservoir (Saunders *et al.* 2008). Moreover, self-potentials have been monitored during hydraulic tests in boreholes leading to some relationship with the microseismicity (Darnet *et al.* 2006), and showing a non-linear behaviour that could be related to the saturation and desaturation processes (Maineult *et al.* 2008). Streaming potential (SP) results from the coupling between fluid (water) flow and electrical current, through the motion of ionic charges of water in the pore space. The distribution of ions near the matrix surface is described by the electric double layer, including the diffuse layer in which the number of counterions exceeds the number of cations adsorbed to the matrix (Davis *et al.* 1978). The streaming current is caused by the motion of ions from the diffuse layer, coming from a pressure difference. This current is then balanced by a conduction current leading to the SP.

In steady state flows through homogeneous media, one can define the SP coefficient C as the ratio between the measured electrical potential difference ΔV and the driving pore water pressure difference ΔP (Overbeek, 1952). The SP is a function of various parameters, and its dependence on water salinity (Ishido & Mizutani 1981; Jaafar *et al.* 2009; Vinogradov *et al.* 2010), water electrical conductivity (Pride & Morgan 1991; Lorne *et al.* 1999), pH (Ishido

& Mizutani 1981; Guichet *et al.* 2006) or temperature (Tosha *et al.* 2003) is still studied.

However, one is forced to note a lack of data concerning the SP coefficient dependence on water content. For shallow surface geophysical applications, including also the seismoelectric conversions (Dupuis *et al.* 2007), which is studied in laboratory (Bordes *et al.* 2006, 2008), a better understanding of electrokinetics for unsaturated conditions is needed. A way for the understanding of such a phenomena is to study the SP coefficient as a function of saturation.

The first experimental SP coefficient measurements were performed by Guichet *et al.* (2003). These authors measured SP during drainage experiments performed by injecting inert gas through sand, and inferred a linear relation between the relative SP coefficient C_r (i.e. C normalized by its value at saturation C_{sat}) and effective water saturation S_e . Perrier & Morat (2000) proposed an empirical expression to explain the dependence of C_r on water content based on a relative permeability model. The implicit assumption was that the electrical currents are affected by unsaturated state in a comparable way than hydrological flow. Revil *et al.* (2007) proposed recently another formula to characterize this dependence also based on a relative permeability model. Linde *et al.* (2007) proposed another expression to model some SP measurements performed during a drainage experiment, with similar conditions to those from Allègre *et al.* (2010). However, these studies do not provide a combined hydrodynamic and electrical approach to model the data, as it should be done. For reservoir applications, Saunders *et al.* (2008) proposed a linear expression for C_r in the case of oil imbibition. All these models predict a monotonous decrease of C_r with decreasing water saturation. Recently, Allègre *et al.* (2010) proposed original SP measurements performed during a drainage experiment and measured the first continuous recordings of the SP coefficient as a function of water saturation. They observed that the SP coefficient exhibits two different behaviours as the water saturation decreases. Values of C_r first increase for decreasing saturation in the range $0.55-0.8 < S_w < 1$, and then decrease from $S_w = 0.55-0.8$ to residual water saturation. This behaviour was never reported before and called for new interpretations of electrokinetic phenomena for unsaturated conditions.

SP signals have been successfully modelled for aquifer properties determination (Darnet *et al.* 2003) or for water infiltration conditions (Sailhac *et al.* 2004). Sheffer & Oldenburg (2007) proposed a 3-D modelling of SP at the field scale for saturated conditions. Jackson (2010) used a bundle capillary model to compute the SP coefficient as a function of water saturation. He showed that the behaviour of the SP coefficient depends on the capillary size distribution, the wetting behaviour of the capillaries and whether we invoke the thin or thick electrical double layer assumption. Depending upon the chosen value of the saturation exponent and the irreducible water saturation, the relative SP coefficient may increase at partial saturation, before decreasing to zero at the irreducible saturation.

Finally, no previous study took into account hydrodynamics and electrical potential equations together, even in a simple geometry, to model the SP coefficient for unsaturated conditions. Thus, we propose here to model SP by solving both the Richards' equation for hydrodynamics and the Poisson's equation for electrical potential using 1-D finite-element method. Existing models which describe the behaviour of C_r as a function of S_e are tested and compared to a new expression inferred from SP measurements by Allègre *et al.* (2010). Thus, after introducing governing equations, computed SP using these models are presented and compared to measurements. The results lead to the conclusions that (1) a non-monotonous

behaviour of C_r is required to fit the measurements and (2) the apparent measurement of $\Delta V/\Delta P$ for the dipoles can provide the SP coefficient in these conditions.

2 GOVERNING EQUATIONS

2.1 Hydrodynamic equations

Combining the mass conservation equation to the 1-D generalized Darcy's law leads to the mixed form of the Richards' equation (Richards 1931), which describes unsaturated flow in porous media

$$\frac{\partial \theta(h)}{\partial t} - \frac{\partial}{\partial z} \left[K(h) \left(\frac{\partial h}{\partial z} - 1 \right) \right] = 0, \quad (1)$$

where $\theta(h)$ is the volumetric water content ($\text{m}^3 \text{m}^{-3}$), dependent on the pressure head h (m). The parameter K , which is also a function of the pressure head, is the hydraulic conductivity (m s^{-1}), t is time (s), and z is the vertical coordinate (m) taken to be positive downward. The dependence of the hydraulic conductivity and pressure head on water content is non-linear. Numerous retention and relative permeability models are able to take into account this dependence (Gardner, 1958; Brooks & Corey 1964; van Genuchten, 1980). The models which have been chosen for this work were proposed, respectively, by Brooks & Corey (1964),

$$S_e = \frac{\theta - \theta_r}{\theta_s - \theta_r} = \begin{cases} \left(\frac{h_a}{|h|} \right)^\lambda, & \text{if } \frac{h_a}{|h|} < 1 \\ 1, & \text{if } \frac{h_a}{|h|} > 1 \end{cases} \quad (2)$$

and Mualem (1976),

$$K(S_e) = K_s S_e^{L+2+\frac{2}{\lambda}}, \quad (3)$$

with S_e the effective water saturation, θ_s the water content at saturation ($\text{m}^3 \text{m}^{-3}$), also equal to porosity ϕ , θ_r the residual water content ($\text{m}^3 \text{m}^{-3}$) and K_s the hydraulic conductivity at saturation (m s^{-1}). The effective water saturation can be expressed by: $S_e = (S_w - S_w^r)/(1 - S_w^r)$, with S_w ($S_w = \theta/\phi$) and S_w^r ($S_w^r = \theta_r/\phi$) the water saturation and the residual water saturation, respectively. The parameter λ in eq. (2) is a measure of the pore size distribution and characterizes the medium granulometry. Thus, higher the value of λ is, higher homogeneous the medium is. The second hydrodynamic parameter h_a is the air entry pressure (Brooks & Corey 1964). The last parameter L takes into account the tortuosity and is chosen as $L = 0.5$, which is a common value in the literature (Mualem, 1976).

Some initial and boundary conditions are necessary to solve the Richards' equation. Initial condition is a saturated sand at the hydrostatic equilibrium, so that the water pressures (expressed in centimetres of water) at the top and the bottom boundary of the system are, respectively, $h(z=0) = 0$ and $h(z=l) = l$. Considering the drainage experiment which will be presented in this work, two conditions have been used. The first one is a zero flux $q_0(t)$ at the top of the system (Neumann type) and the second one is a constant pressure head $h_l(t)$ at the bottom (Dirichlet type). These conditions are written as

$$h(z=l, t) = h_l(t) \text{ and } \left(-K(h) \frac{\partial h}{\partial z} + K \right)_{z=0} = q_0(t), \quad (4)$$

where $z=0$ or $z=l$ and l the length of the system. The Richards' equation has been discretized using the Galerkin finite-element method (Pinder & Gray 1977), with a fully implicit scheme in time. To take into account dependency between h , θ and K , the equation is linearized using the Newton-Raphson method. This approach has been used for decades to solve this equation, and the

detailed scheme can be found, for example, in Lehmann & Ackerer (1998).

2.2 Electrokinetic theory

Coupled fluxes can be described by the general equation

$$\mathbf{J}_i = \sum_{j=1}^N \mathcal{L}_{ij} \mathbf{X}_j, \quad (5)$$

which link the forces \mathbf{X}_j to macroscopic fluxes \mathbf{J}_i , through transport coupling coefficients \mathcal{L}_{ij} (Onsager 1931). The global SP field can be described as the sum of several contributions creating electrical current sources. These current sources derive from macroscopic potentials, through electrochemical effects (e.g. concentration gradients), electrokinetics (e.g. electrical potential gradients and electro-osmosis) or thermoelectrical effects (e.g. temperature gradients). Considering some of these potential fields, the total electrical current density can be written as

$$\mathbf{J} = -\mathcal{L}_T \frac{\nabla T}{T} + \nabla \Phi_J + \mathcal{L}_e \nabla V - \mathcal{L}_{ek} \nabla P, \quad (6)$$

where T is the temperature (K), $\mathcal{L}_T = -T\pi\sigma_T$ (W m s⁻¹) is given by the Peltier effect, Φ_J is the junction potential (V), which also can be expressed as a function of chemical concentration gradients in electrolytes ($\nabla C_c/C_c$) by $\nabla \Phi_J = \alpha_m \nabla C_c/C_c$, with α_m the fluid junction coupling coefficient (Naudet *et al.* 2003; Mainault *et al.* 2008; Jouniaux *et al.* 2009). The parameter V is the electrical potential (V), thus Ohm's law identify $\mathcal{L}_e = -\sigma_r$, with σ_r the bulk electrical conductivity (S m⁻¹). The last term of eq. (6) describes electrokinetic effects created by the driving pressure gradient ∇P , through the electrokinetic coupling \mathcal{L}_{ek} , defined as $\mathcal{L}_{ek} \equiv -\sigma_r C$ (A Pa⁻¹ m⁻¹) (Pride, 1994). The parameter C (V Pa⁻¹) is known as the SP coefficient. The total water pressure P can be inferred from water pressures h with: $P = \rho_w g(h - z)$, where ρ_w is the water density (kg m⁻³), g is gravity and z is the vertical location taken to be positive downward.

Considering a constant temperature, and no concentration gradients, one can write the following coupled equation:

$$\mathbf{J} = \mathcal{L}_e \nabla V - \mathcal{L}_{ek} \nabla P, \quad (7)$$

or

$$\mathbf{J} = -\sigma_r \nabla V + \sigma_r C \nabla P. \quad (8)$$

Without any external current sources, the conservation of the total current density implies

$$\nabla \cdot \mathbf{J} = 0. \quad (9)$$

In the case of heterogeneous medium, one can assume, for example, a tabular medium with electrical conductivity and SP coefficient contrasts, then eqs (8–9) leads to the following Poisson's equation:

$$\nabla \cdot \mathbf{J} = -\sigma_r \nabla^2 V - \nabla V \cdot \nabla \sigma_r + \nabla(C\sigma_r) \cdot \nabla P + \sigma_r C \nabla^2 P = 0. \quad (10)$$

In addition to primary current sources occurring from the term $\sigma_r C \nabla^2 P$, some secondary sources linked to the term $\nabla(C\sigma_r) \cdot \nabla P$ appear. These sources are located at boundaries formed by electrical conductivity and SP coefficient contrasts.

In the case of an homogeneous medium and without any contrasts of σ_r and C , eq. (10) reduces to

$$\nabla^2 V = C \nabla^2 P. \quad (11)$$

Considering, for example, a steady-state saturated flow through a capillary, the SP coefficient C (V Pa⁻¹) can be expressed as the ratio between the SP difference ΔV (V) and the driving-pressure difference ΔP (Pa)

$$C = \frac{\Delta V}{\Delta P}. \quad (12)$$

In 1-D, eq. (9) can be written as

$$\frac{\partial}{\partial z} \left(-\sigma_r \frac{\partial V}{\partial z} \right) + \frac{\partial}{\partial z} \left[\rho_w g \mathcal{L}_{ek} \left(\frac{\partial h}{\partial z} - 1 \right) \right] = 0. \quad (13)$$

2.3 Discretization of the Poisson's equation

The Poisson's equation was solved using 1-D finite-element method. A first-order basis function $\phi(z)$ has been chosen to discretize the Poisson's equation. This choice implies that variables and coefficients of eq. (13) vary linearly in each element. For each node i of the system, the basis function is written $\phi_i(z)$. Then, the equation which has to be solved can be written as

$$\int_0^l \frac{\partial}{\partial z} \left(-\sigma_r \frac{\partial V}{\partial z} \right) \phi(z) dz + \int_0^l \frac{\partial}{\partial z} \left[\rho_w g \mathcal{L}_{ek} \left(\frac{\partial h}{\partial z} - 1 \right) \right] \phi(z) dz = 0. \quad (14)$$

Using this method, all variables and coefficients are approximated on each element using the same basis function

$$V(z, t) = \sum_1^{ne} V_i(t) \phi_i(z), \quad (15)$$

$$h(z, t) = \sum_1^{ne} h_i(t) \phi_i(z), \quad (16)$$

$$\mathcal{L}_{ek}(z, t) = \sum_1^{ne} \mathcal{L}_{eki}(t) \phi_i(z), \quad (17)$$

$$\sigma_r(z, t) = \sum_1^{ne} \sigma_{ri}(t) \phi_i(z), \quad (18)$$

where $nn = ne + 1$ is the number of nodes in the system of length l and ne the number of elements. The $V_i(t)$, $h_i(t)$, $\mathcal{L}_{eki}(t)$ and $\sigma_{ri}(t)$ are, respectively, the values of the electrical potential, water pressure, electrokinetic coupling and bulk electrical conductivity at node i . For notations simplicity, $\mathcal{L}_{eki}(t)$ will be written $\mathcal{L}_i(t)$ in the following. After integrating by parts eq. (14), the final system of equation to be solved is given by

$$[A] \cdot V_i = -[B] h_i - \{F_j\}, \quad (19)$$

where the elements of $[A]$, $[B]$ and vector $\{F_j\}$ can be deduced from the following integrals:

$$A_{ij} = \int_0^l \left(\sum_{k=1}^{nn} \phi_k \sigma_k \right) \phi'_i \phi'_j dz, \quad (20)$$

$$B_{ij} = \rho_w g \int_0^l \left(\sum_{k=1}^{nn} \phi_k \mathcal{L}_k \right) \phi'_i \phi'_j dz, \quad (21)$$

$$F_j = \rho_w g \int_0^l \left(\sum_{k=1}^{nn} \phi_k \mathcal{L}_k \right) \phi'_j dz. \quad (22)$$

The matrix $[A]$ is tridiagonal and the system can be solved using Thomas algorithm (Press *et al.* 1992). The system introduced in eq. (19) can be detailed for each element i as

$$\begin{aligned} \frac{1}{2\Delta z} [-(\sigma_{i-1} + \sigma_i)V_{i-1} + (\sigma_{i-1} + 2\sigma_i + \sigma_{i+1})V_i \\ - (\sigma_i + \sigma_{i+1})V_{i+1}] = \frac{\rho_w g}{2\Delta z} [(\mathcal{L}_{i-1} + 2\mathcal{L}_i) + \mathcal{L}_{i+1})h_i \\ - (\mathcal{L}_{i-1} + \mathcal{L}_i)h_{i-1} - (\mathcal{L}_i + \mathcal{L}_{i+1})h_{i+1} + (\mathcal{L}_{i-1} + \mathcal{L}_{i+1})], \end{aligned} \quad (23)$$

where $\Delta z = 0.1$ cm is the spatial discretization. Boundary conditions at nodes 1 and nn are

$$\sigma_1 \frac{\partial V}{\partial z} \phi_1 = -j_0, \quad (24)$$

$$\sigma_{nn} \frac{\partial V}{\partial z} \phi_{nn} = -j_i, \quad (25)$$

with j_0 and j_i are the values of the current density at the top and the bottom of the system, respectively. The Poisson's equation is solved in terms of electrical potential V . Thus, two boundary conditions are necessary: one on the total current density J (Neumann type) and one on the electrical potential itself V (Dirichlet type). As no current outflow can occur at the top and the bottom of the system (i.e. no electrical exchange between the medium and the air), the total current density j_0 at $z = 0$ and $z = l$ are: $j_0 = j_l = 0$ A m⁻². In addition, a constant value of electrical potential V_0 has been chosen at the top of the system. This constant can be a reference value, so that $V_0 = 0$ V has been chosen for simplicity.

The modelling process is carried out using the following protocol: (1) Considering hydrodynamic boundary conditions, eq. (1) is first solved, so that water pressures and corresponding water contents are computed at each node and each time step; (2) The Poisson's equation is then solved using eq. (19), which allows to compute the electrical potential at each node of the system and (3) Thus, the needed potential differences can be deduced from the computed electrical potential field and compared to measurements. The next section presents a test performed considering a linear water pressure profile in saturated conditions, that is, simulating a Darcy's experiment. The following sections go into the unsaturated case and present computed SP differences and measurements in the case of a drainage experiment. Several hypotheses on SP coefficient dependence on water content will be considered and compared.

3 SATURATED FLOW MODELLING

The first step is to test the code accuracy by modelling a saturated flow through a column of sand ($l = 1.16$ m height), that is, a Darcy's experiment. The complete scheme described earlier was applied, so that eqs (1) and (10) were solved. The water electrical conductivity σ_w and saturated SP coefficient C_{sat} corresponding to this test are those of Allègre *et al.* (2010) and are reported in Table 1. A linear and steady-state water pressure profile was applied to the medium (Fig. 1a). Thus, boundary conditions at the top and the bottom of the column are constant water pressure head and given by:

Table 1. Parameters used to perform the Darcy's experiment simulation, deduced from Allègre *et al.* (2010).

σ_w (S m ⁻¹)	C_{sat} (V Pa ⁻¹)	h_0 (cm H ₂ O)	h_l (cm H ₂ O)
103.2×10^{-4}	-1.6×10^{-6}	20	60

$h_0(t) = 20$ cm and $h_l(t) = 60$ cm. In this case, the medium remains saturated, so that $S_w = 1$. The boundary conditions for Poisson's equation was a zero current density J_0 at the top and a constant electrical potential $V_0 = 0$ V at the bottom of the column. The first simulated electrode (#10) is located at 11 cm from the top of the system, whereas other electrodes are placed each 10 cm along it. The SP are then computed between the first five electrodes (#10 to #6) and the reference electrode (#1 15 cm above column's bottom) and for each dipole formed by two consecutive electrodes (e.g. $\Delta V_{10,9}$ will be the computed electrical potential difference between electrodes #10 and #9). The simulation were performed for 200 hr, and the same results were obtained at each time step.

The SP differences computed between each electrode and the reference are different. This is coherent with the increasing size of each dipole, so that larger the dipole is, larger the SP difference is (Fig. 1b). As the medium is homogeneous (fully saturated), SP differences computed for each dipole are merged (Fig. 1c) and exhibit the value $\Delta V_{i,i-1} = -0.0954$ mV. The corresponding driving pore pressure difference for each dipole is $\Delta P_{i,i-1} = 59.67$ Pa. Considering these values, the inferred SP coefficient at saturation computed with eq. (12) is $C_{sat} = -1.6 \times 10^{-6}$ V Pa⁻¹. This value is exactly equal to the original C_{sat} (see Table 1) used for calculation. This test experiment was performed using others water pressure profiles, other C_{sat} values and other boundary condition value V_0 and always yielded to the original C_{sat} . We therefore confirm that the apparent measurement of $\Delta V/\Delta P$ for the dipoles can provide the SP coefficient for saturated conditions.

4 DRAINAGE EXPERIMENT

4.1 Unsaturated flow modelling

We propose to model the SP measurements of a drainage experiment carried out by Allègre *et al.* (2010). The SP were measured during a drainage experiment performed in a column of plexiglass of approximately 1.2 m height and 10 cm diameter fulfilled with clean Fontainebleau sand. A constant water pressure applied at the bottom of the column allowed the drainage to start. Allègre *et al.* (2010) combined SP measurements to water content and water pressure measurements each 10 cm along the column. The aim of this section is to computed SP using the numerical scheme described earlier, considering several hypotheses for the SP coefficient dependence on water content. Thus, formula for C_r of Guichet *et al.* (2003), Revil *et al.* (2007) and a new empirical model will be implemented to solve the Poisson's equation.

At the beginning of the experiment, the medium is fully saturated, so that the water pressure profile is hydrostatic. The drainage starts when the boundary condition at the bottom of the column is set to a value of $h = 2$ cm of equivalent water height (i.e. $p_w(z = l) \simeq 200$ Pa). The water pressure heads and water contents are computed at each time step by solving eq. (1) and are compared to experimental data (Fig. 2). The parameters of the retention model (eq. 2) and the relative permeability model (eq. 3) are reported in Table 2. Since pressure sensors are located each 10 cm along the column, before the drainage start, the pressure heads measurements are shifted from 10 cm between each other. These measurements are characteristics for the hydrostatic equilibrium. After the drainage start, the measured pressure heads decrease all at the same time and stabilize at different values depending on the sensor location. This shift of the pressure values at the end of the experiment (e.g. at $t \simeq 150$ hr) indicates the presence of a capillary fringe and of a water

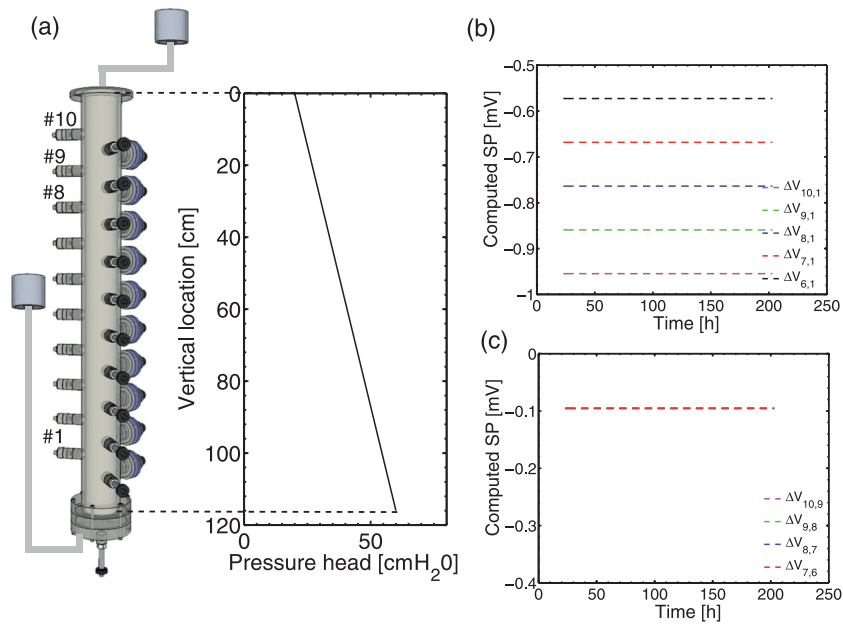


Figure 1. (a) The water pressure profile used for the Darcy's experiment simulation. The pressure head boundary conditions are constant and equal to $h_0 = 20$ cm and $h_l = 60$ cm of equivalent water height at the top and the bottom of the column, respectively. (b) Computed SP between the first five electrodes (#10 to #6) and the reference #1. (c) Computed SP for the dipoles (10,9), (9,8), (8,7) and (7,6). The computed values are $\Delta V_i, i - 1 = -0.0954$ mV and $\Delta P_i, i - 1 = 59.67$ Pa which lead to $C_{\text{sat}} = 1.6 \times 10^{-6}$ V Pa⁻¹.

saturation gradient (see Fig. 2b). For very long time (around 90 d for the sand used), the water phase equilibrates itself in the column until a linear water pressure profile is reached. From the drainage start, the water saturations do not decrease at the same time, but one after the other depending on the measurement location. The time-shift between the water content measurements informs on the dynamic of the saturation front propagation during the drainage experiment.

The hydrodynamic parameters used in the Richards' equation (Table 2) were computed by inversion of the water pressure heads and water content measurements. The detailed inverse problem procedure can be found in Hayek *et al.* (2008). It is shown that this approach provides good estimations and small errors on θ_s , λ and h_a .

4.2 Unsaturated SP modelling

To solve the Poisson's equation at each time step, a model for the SP coefficient dependence on water saturation is needed. Guichet *et al.* (2003) proposed that the SP coefficient vary linearly with the effective water saturation

$$C_r = S_e. \quad (26)$$

Revil *et al.* (2007) had a different approach and proposed another relation depending on a relative permeability model as

$$C_r = \frac{k_r}{S_w^{n+1}} \text{ with } k_r = S_e^{L+2+2/\lambda}, \quad (27)$$

where n is the Archie's saturation exponent (Archie 1942). The L parameter is usually chosen as $L = 0.5$ (Mualem, 1976), but is equal to 1 in Revil *et al.* (2007), so that the two cases will be tested in the following. These two models have in common to predict the maximum of the SP coefficient to be C_{sat} (for $S_w = 1$). Moreover, they imply a monotonous decrease of the relative SP coefficient with decreasing saturation. Allègre *et al.* (2010) recently observed that C_r could be until 200 times larger than C_{sat} , and that it first

increases with decreasing saturation, and then decreases up to the residual water saturation. So that, we propose an empirical relation for the SP coefficient inferred from these measurements written as

$$C = C_{\text{sat}} S_e [1 + \beta(1 - S_e)^\gamma], \quad (28)$$

where β and γ are two fitted parameters. Note that β depends on the considered dipole and varies as a function of the vertical location. This assumption coming from the experimental SP coefficients, which exhibit different maximum values, will be discussed in the following section. Contrary to the two first relations, this model predicts a non-monotonous behaviour of the SP coefficient as a function of water saturation. The three presented models were used to compute $C(S_e)$ from computed water saturations, to solve the Poisson's equation.

Moreover, an *a priori* is needed for the electrical conductivity $\sigma_r(S_w)$ to solve eq. (10). The electrical conductivity is inferred at each time step using the Archie's law (Archie 1942)

$$\sigma_r = \sigma_w \phi^m S_w^n, \quad (29)$$

with m and n the two Archie's exponents, σ_w the water electrical conductivity (S m⁻¹) and ϕ the porosity. The relation $C(S_e)$ is also computed at each time step and for each element of the system from computed water saturations. All parameters' values needed for computation are reported in Tables 2 and 3. Using the computed electrical potential values in the column, SP were computed for the dipoles (10,9), (9,8), (8,7) and (7,6), which are the dipoles located in the unsaturated part of the column during the drainage experiment.

5 DISCUSSION

The SP were computed solving eqs (1) and (10) for the three presented models (Fig. 3). The computed SP using Guichet *et al.* (2003) and Revil *et al.* (2007) models are very small compared to the measurements (Figs 3a and b). A jump, corresponding to the drainage start, is observed in SP signals at the beginning of the simulation.

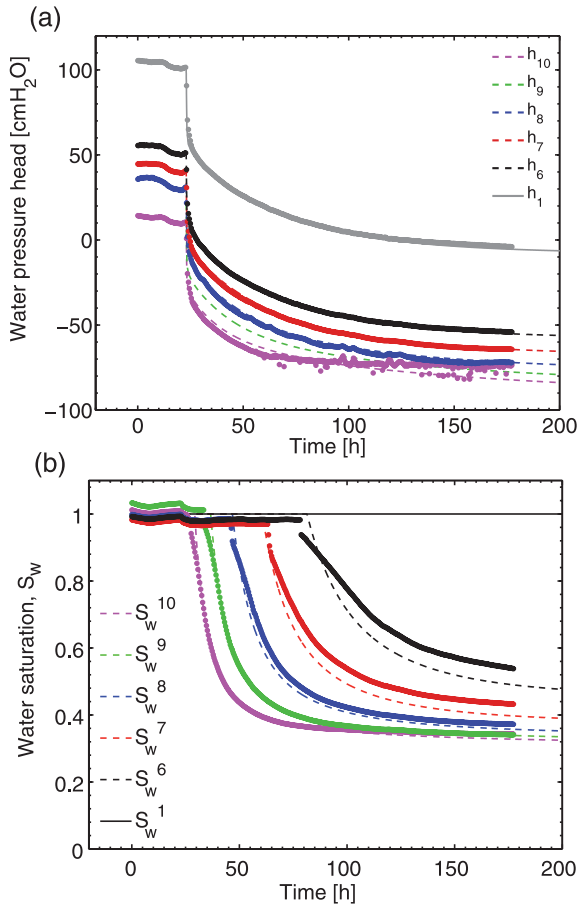


Figure 2. (a) Measured (dots) and computed (dashed lines) water pressure heads deduced from the Richards' equation solving. Index i indicates the location of measurement, as h_{10} is the pressure head 16 cm from the column top and h_1 10 cm from the column bottom. Other h values are measured and computed each 10 cm. (b) Measured (dots) and computed (dashed lines) water saturations deduced from the Richards' equation solving, where index i indicates the location of measurement. The drainage starts at $t \approx 22$ hr.

Its magnitude is around 0.09 mV for tests performed using eqs (26) and (27) and is the same for all dipoles (Figs 3d and e). In the case of Guichet *et al.* (2003) model (Fig. 3d), the computed SP begin to decrease to reach a minimum value for dipoles (10,9) and (9,8) around -0.11 mV and then increase. This minimum is observed at the time when water saturation stops to decrease for all dipoles. In the case of Revil *et al.* (2007) model, the increasing of computed SP is monotonous during the simulation, from a value around -0.09 mV to almost 0 for all dipoles. It is obvious that these two models are not appropriate to explain the SP measurements both in terms of magnitude and behaviour.

Revil *et al.* (2007) used $L = 1$ in their model, instead of $L = 0.5$ as proposed by Mualem (1976) to hold as the best value for 45 soils including sand. Consequently, eq. (27) was also implemented using $L = 0.5$, which leads to a modified Revil *et al.* (2007) model. The

Table 3. Parameters needed to implement eqs (27)–(29) in the Poisson's equation. The four values given for β corresponds to the dipoles from (10,9) to (7,6). The n value was measured in (Allègre *et al.* 2010).

C_{sat} (V Pa ⁻¹)	σ_w (S m ⁻¹)	n (Archie's exponent)	β	γ
-1.6×10^{-6}	103.2×10^{-4}	1.45	32,52,72,92	0.4

results (Fig. 3e) are similar to those for $L = 1$ in terms of amplitude, but show an increasing of SP signals without any step as it was observed before. The choice of L is quite important because it is involved in the global power law in eq. (27), and consequently influences the shape of the model (Allègre *et al.* 2010).

On the other hand, the model introduced for C_r by eq. (28) leads to good results in terms of computed SP. The measured SP signals are well reproduced, particularly at the beginning of the experiment between $t \approx 20$ hr and $t \approx 100$ hr. The computed SP corresponding to dipoles (10,9) to (7,6) decrease one after the other when water saturation (measured at the same level) begins to decrease (see Figs 2b and 3c). Thus, the saturation front propagation is characterized by the time-shift between SP decreasing starts. The computed SP using both eqs (26) and (27) are up to one and a half order of magnitude smaller than those computed using expression (28) (Fig. 3).

For times over 100 hr, the residuals between measured and computed SP are larger. At this point of the experiment, the water flow is very low, leading to very small variations of SP. This point is interpreted in Allègre *et al.* (2010), who precise that for such low water outflow (even not measurable), the SP variations are too weak to insure robust interpretation. Consequently, a better fit was expected at the beginning of the experiment (when the water flow is maximum), which is the case for three measurement dipoles. In addition, all the tests performed to ensure the quality of SP recordings and prevent the external sources of noise from disturbing the measurements, including a statistical study on uncertainties, can be found in Allègre *et al.* (2010, appendices A and B). Moreover, the fit and estimation of the set of parameters of eq. (28) would be improved if the SP measurements were inverted. Thus, a joint inversion would give more informations on parameters sensitivities.

One can verify the assumption made by Allègre *et al.* (2010) to use eq. (12) to the inferred SP coefficients from SP measurements. Thus, SP coefficients were computed using eq. (12), and compared to SP coefficients computed with eq. (28) averaged on 10 cm to be representative of the same investigated volume (Fig. 4). It is shown that SP coefficients using eqs (12) and (28) give very close results in terms of behaviour and magnitude. This example prove the validity of using eq. (12) to infer accurate values of C even for non-steady conditions. One can consider that these values are apparent SP coefficients because the water saturation distribution is not perfectly homogeneous in 10 cm of sand, however, they are still perfectly representative of true SP coefficients, at least for this kind of drainage experiment.

Furthermore, computed SP coefficients using different assumptions for C_r (eqs 26–28) can be compared to measurements of $\Delta V / \Delta P$ from Allègre *et al.* (2010, Fig. 5). The fitted values of β , γ and parameters of eqs (26) and (27) are reported in Table 3. It is clear

Table 2. Hydrodynamic parameters values used to solve the Richards' equation for unsaturated conditions. The parameter K_s^{meas} is the measured permeability of the sand. These two values of permeability lead to the same results for pressure and water-content behaviours.

K_s ($\times 10^{-5}$) (m s ⁻¹)	K_s^{meas} ($\times 10^{-5}$) (m s ⁻¹)	h_a (m)	λ	θ_r (–)	θ_s, ϕ (–)	S_w^r (–)
1.65	17.2	0.4	3.88	0.11	0.36	0.305

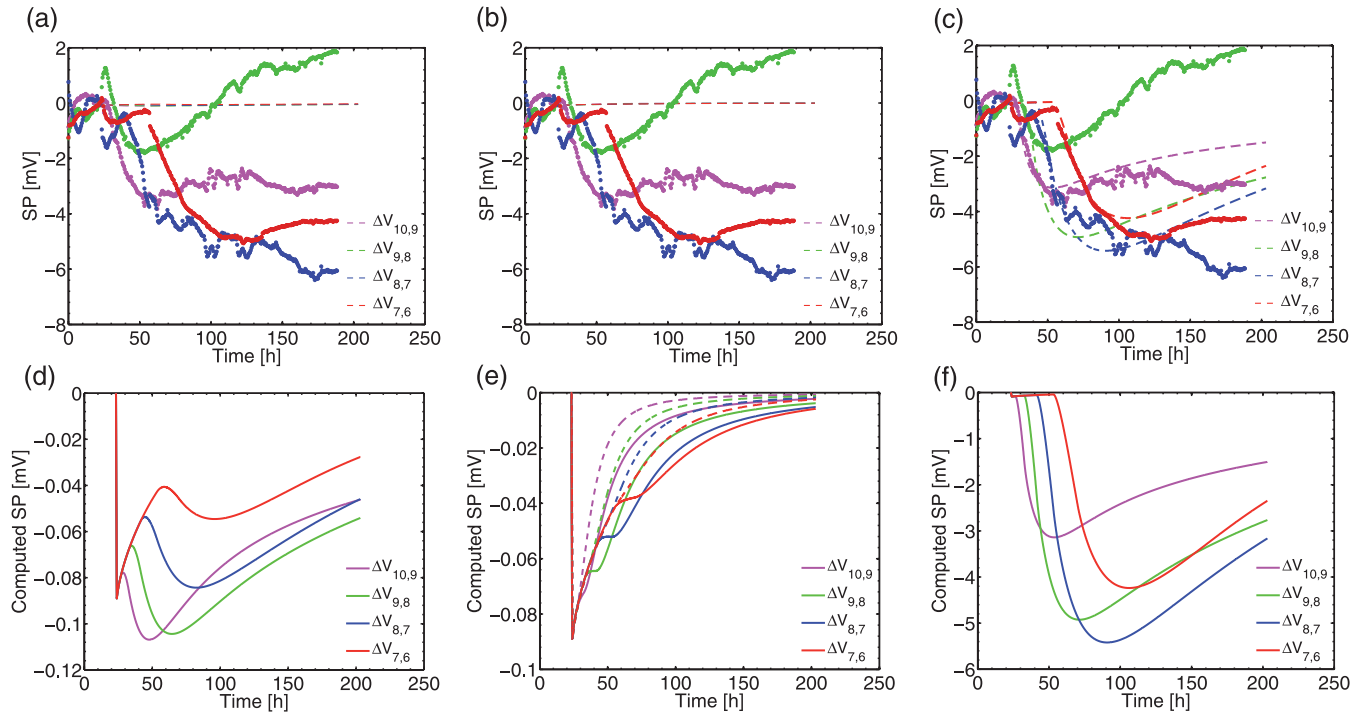


Figure 3. Measured (dots) and computed (lines) streaming potentials deduced from the Poisson's equation solving, for each dipole, using, respectively, eqs (26) (a), (27) (b) and (28) (c). Computed SP using eqs (26) (d), (27) (e) and (28) (f) in the Poisson's equation, and parameters from Tables 2 and 3. The Revil et al. (2007) model (e) has been implemented using $L = 0.5$ (lines) and $L = 1$ (dashed lines).

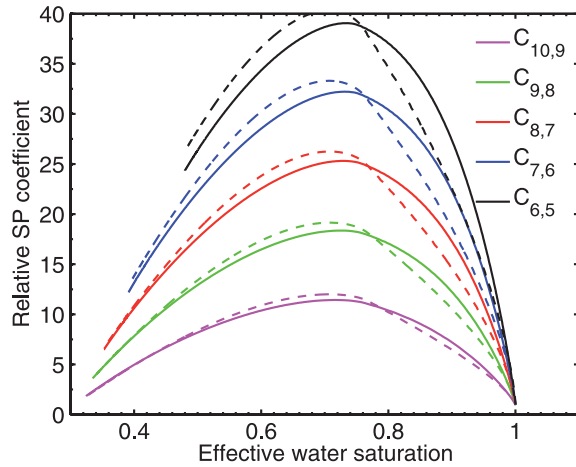


Figure 4. Computed relative SP coefficients using eq. (12) with computed ΔV and ΔP after Poisson's equation was solved (lines), and using eq. (28) (dashed lines), for five locations in the column.

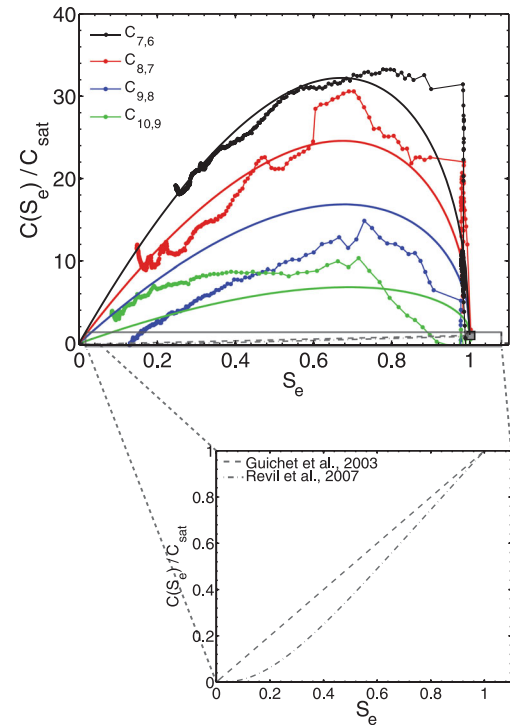


Figure 5. (Top panel) Experimental SP coefficients $\Delta V/\Delta P$ from Allègre et al. (2010) (dots) and model adjusted to measurements using eq. (28). The β and γ values are reported in Table 3. (Bottom panel) The Guichet et al. (2003) and Revil et al. (2007) models for the relative SP coefficient C_r as a function of water saturation.

in Fig. 5 that the two existing models for C_r predict lower values of C_r than measurements and fail to provide the correct behaviour of C_r . Moreover, the measured SP coefficients $\Delta V/\Delta P$ are quite well reproduced in the case of using eq. (28). It is important to note that Allègre *et al.* (2010) inferred experimental SP coefficients using eq. (12), which is classically used for steady-state flows, neglecting electrokinetic sources coming from SP coefficient and electrical conductivity contrasts. Since no electrokinetic sources have been

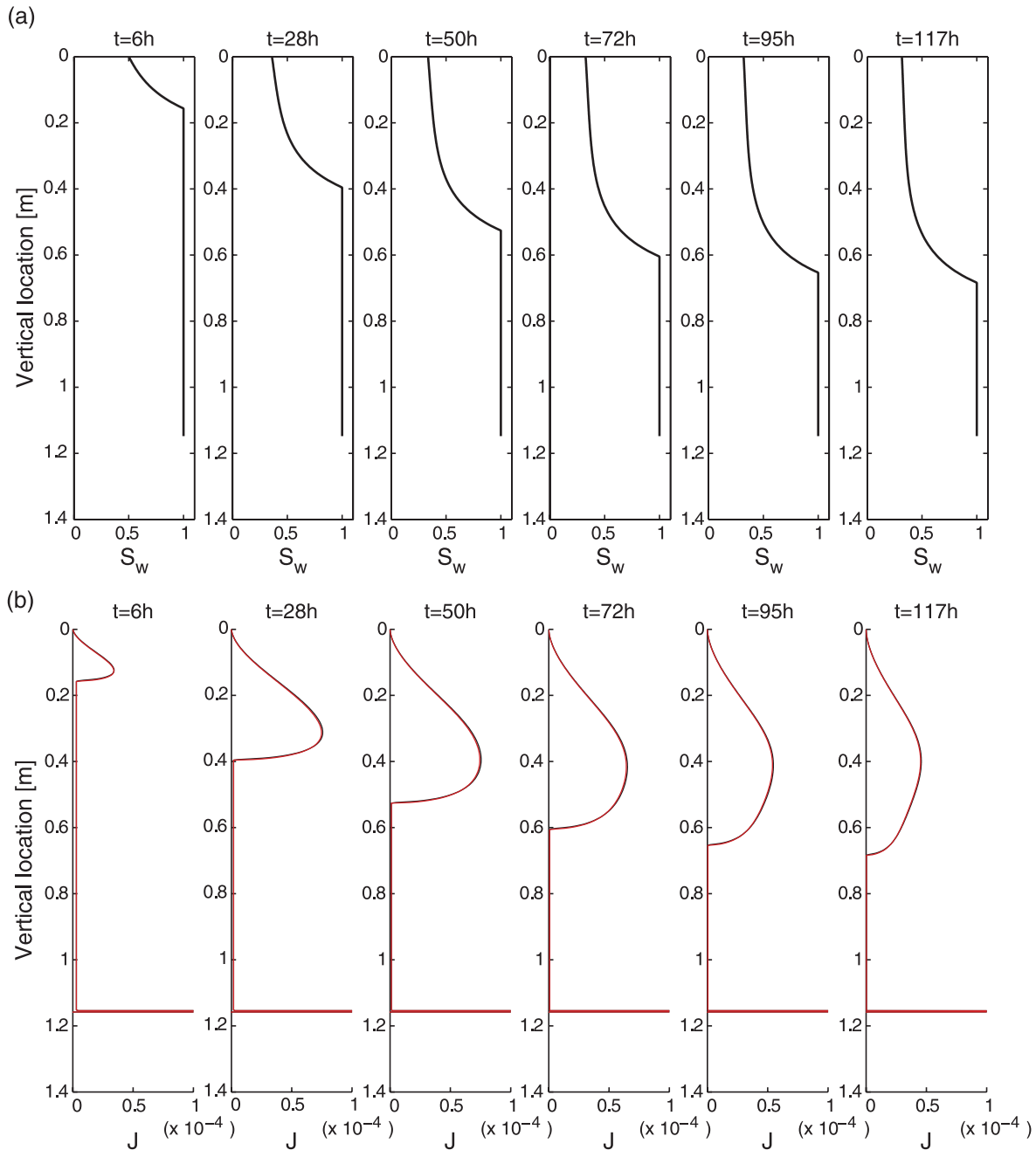


Figure 6. Snapshots of the water saturation profile (a) and total current density components J_{cond} (black line) and J_{conv} (red line), b) for six times between $t = 6$ hr and $t = 117$ hr. The electrical current density is expressed in A m^{-2} . The snapshot corresponds to the simulation performed using eq. (28) for implementation of $C(S_e)$ in the Poisson's equation.

neglected in the present modelling, one can conclude that the non-monotonous behaviour combined to large values of C_r observed previously are not artefacts and are not created by neglected contrasts of C_r or σ_r but has a physical origin. Therefore, we show that the measurement of apparent $\Delta V / \Delta P$ for the dipoles can provide the SP coefficient C_r in these conditions. Nevertheless, a slight difference is observed between the maximum of computed and measured SP coefficients. These differences come from the use of eq. (12) to infer SP coefficients. Finally, these results confirm that a different maximum in C_r for each dipole is necessary to provide accurate computed SP differences. We suggest that this observation has a physical meaning coming from the flow behaviour. Indeed, each

dipole is not affected by the same hydrodynamic conditions, and particularly the same flow velocity, when water saturation (at its level) decreases.

An important point to discuss is the behaviour of the total current density. Fig. 6 shows six snapshots of both water saturation and current density component $J_{\text{cond}} = -\sigma_r \nabla V$ and $J_{\text{conv}} = \sigma_r C \nabla P$ vertical profiles at six time during the simulation. The components J_{cond} and J_{conv} are computed *a posteriori* using finite differences. Even if SP sources are linked to $\nabla \cdot \mathbf{J}$, as introduced by the conservation equation (eq. 9), we think that the vertical component of \mathbf{J} is still relevant to describe the general behaviour of SP signals. This representation is useful *a posteriori* to interpret the global SP

variations, as it integrates all electrokinetic sources coming from SP coefficient or electrical conductivity contrasts (see eq. 10). The water saturation vertical profiles characterize the propagation of saturation front during the drainage. In the saturated part of the column, $\theta = \theta_s$ thus $S_w = 1$. In the unsaturated part, the saturation decreases from the top to the saturation front. The saturation value at the top of the system decreases during drainage from $S_w(z=0) = 0.5$ at $t = 6$ hr to $S_w(z=0) = 0.33$ at $t = 50$ hr and then stabilizes. For times greater than $t = 50$ h, the water saturation is almost constant ($S_w \simeq 0.33$) for $0 < z < 40$ cm. Moreover, it is shown in Fig. 6(b) that the conduction (J_{cond}) and the convection (J_{conv}) component of the total current density J are almost equal in absolute terms in the whole system during the entire experiment. The maximum difference observed between computed J_{cond} and J_{conv} does not exceed 2 per cent. This is a crucial point because the relation $J_{\text{cond}} = J_{\text{conv}}$ allows the use of eq. (12) (i.e. $C = \Delta V / \Delta P$) to deduce SP coefficient values from measurements. This is another confirmation that this approach can be used and gives accurate results for this kind of experimental conditions.

A large discontinuity is observed at the bottom of the column. This comes from the important contrast of electrical conductivity between the saturated medium and the water in the reservoir at the bottom of the column. Thus, the electrical conductivity changes from $\sigma_{\text{sat}} \simeq 0.002 \text{ S m}^{-1}$ to $\sigma_w = 0.01 \text{ S m}^{-1}$ at this boundary. This is the only possible source of current since the SP coefficient is zero in water. Nevertheless, this contrast does not influence the SP measurements, since the measurements are located far from it and

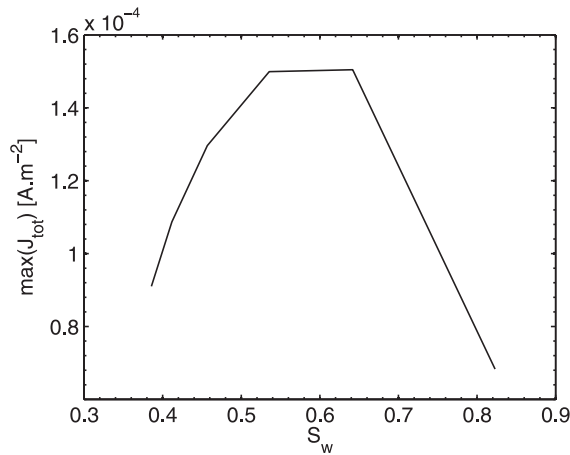


Figure 7. Maximum of the total current density J (black line) inferred from curves in Fig. 6 and corresponding water-flow velocity (dashed black line).

that the current density returns to a constant value in the centimetre above it. It was suggested by Linde *et al.* (2007) and Revil & Linde (in press), that this contrast could be responsible for the behaviour of the measured SP. However, it is not the case for our experiment but may occur for measurements involving an electrode very close to this source. It should be then considered as an experimental artefact in this case.

The second point is that the maxima of J_{cond} and J_{conv} are not located at the higher gradient of water saturation (at the saturation front), corresponding to the higher contrast of electrical conductivity σ_r , but backward from this front. Its absolute value varies not linearly from $3 \times 10^{-5} \text{ A m}^{-2}$ to $6.8 \times 10^{-5} \text{ A m}^{-2}$ for $6 < t < 117$ hr (Fig. 7). This suggests that the predominant contribution to the total electrical density comes from contrasts in SP coefficient which is larger for $S_w \simeq 0.8$ than for saturated conditions. This is obviously a consequence of the behaviour of C_r as a function of water saturation. Thus, it seems that the electrokinetic response could be dominated by SP coefficient gradients and not by electrical conductivity gradients for such water flow.

This statement can be investigated using different parameters in the Archie's law (eq. 29) to increase the influence of the electrical conductivity. Thus, the previous value of $n = 1.45$ is replaced by a larger value as $n = 2.5$. The influence of the saturation exponent n depends on the considered model for the SP coefficient (Figs 8a–c). Indeed, any change in n does not influence the computed SP in the case of using eqs (26) or (28) for calculation. On the contrary, the increasing of n from 1.45 to 2.5 changes both the behaviour and magnitude of computed SP when eq. (27) is implemented (Fig. 8b). Thus, resulting SP exhibit larger values than the previous ones. This is explained by the increasing of the SP coefficient value implied by the increasing of n (see eq. 27). It suggests that electrical conductivity contrasts are insignificant on the computed SP compared to other electrokinetic sources induced by SP coefficient contrasts.

One can conclude that a non-monotonous behaviour combined to large values of $C(S_w)$ needs to be implemented in the Poisson's equation to obtain computed SP close from the measured one. Nevertheless, the expression presented in this work is not sufficient and our approach does not deal with physical considerations. In future work, the water-flow conditions of the drainage experiment and especially the pressure dynamic and flow velocity could be involved in the observed SP coefficient behaviour.

6 CONCLUSIONS

We presented in this work the first modelling of both Richards' and Poisson's equations for unsaturated conditions using 1-D

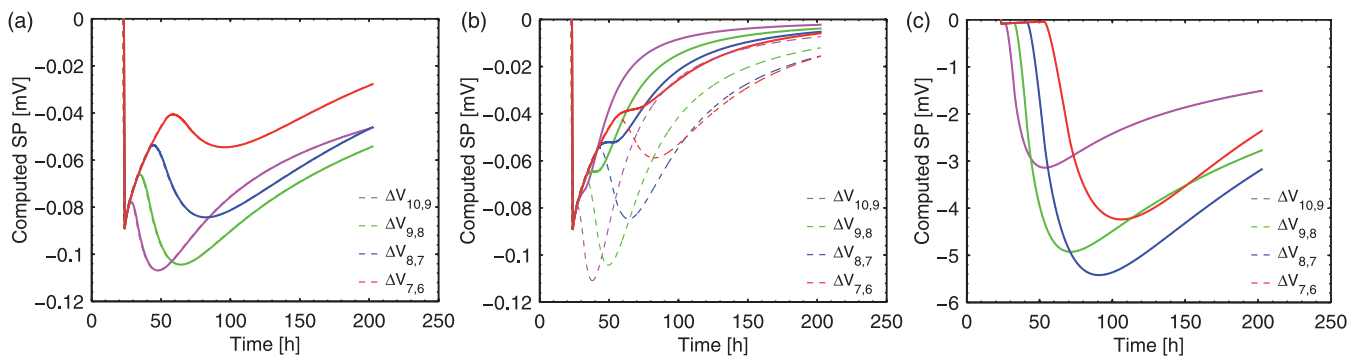


Figure 8. Computed SP (lines) using eqs (26) (a), (27) (b) and (28) (c) with $n = 1.45$, compared to computed SP with $n = 2.5$ (dashed lines).

finite-element method. Several simulations have been performed using three different hypotheses on the SP coefficient C_r to deduce SP differences which have been compared to observations from Allègre *et al.* (2010). The two existing models from Guichet *et al.* (2003) and Revil *et al.* (2007) were not able to predict SP differences consistent with the measurements of Allègre *et al.* (2010), although no electrical current sources have been neglected. We proved with this modelling approach that a non-monotonous expression for $C(S_e)$ is necessary to correctly reproduced these measurements. We also demonstrated the consistency of our SP coefficient data set verifying the equality $J_{\text{cond}} = J_{\text{conv}}$, and consequently the possibility to use the apparent $\Delta V/\Delta P$ measurements to infer correct C values for this kind of drainage experiment. This conclusion has to be verified for other flow conditions, for example, steady-state unsaturated flow conditions with various flow velocities using different sands.

Finally, a joint inversion approach of hydrodynamics and electrical potential, which could improve the modelling results of SP, is undergoing. This approach will help to insure the robustness of our model for long times and will define precisely the sensitivities of inverted model parameters.

For field applications, even if a good correlation can be observed between SP response and precipitation occurrence (Thony *et al.* 1997; Doussan *et al.* 2002), it seems that a linear relationship between water flux and electrical potential gradient would be difficult to establish. Indeed, non-linear effects coming from the behaviour of the SP coefficient for unsaturated conditions, show that this relationship is probably more complex. Moreover, some acquisition issues and changing soil conditions during long experiments make SP difficult to interpret (Doussan *et al.* 2002). However, shorter artificial infiltration experiments using SP monitoring could still be possible at the field scale. SP could be modelled with our new model of relative SP coefficient taking into account for infiltration and/or evaporation with time-varying upper boundary conditions. These experiments could be very useful to infer some hydrodynamic parameters of soils, such as hydraulic conductivity, and give a way to measure ground water flux in the vadose zone.

ACKNOWLEDGMENTS

This work was supported by the French National Scientific Centre (CNRS), by ANR-TRANSEK, and by REALISE, the Alsace Region Research Network in Environmental Sciences in Engineering and the Alsace Region.

REFERENCES

- Allègre, V., Jouniaux, L., Lehmann, F. & Sailhac, P., 2010. Streaming potential dependence on water-content in Fontainebleau sand, *Geophys. J. Int.*, **182**, 1248–1266.
- Archie, G.E., 1942, The electrical resistivity log as an aid in determining some reservoir characteristics, *Trans. Am. Inst. Min. Metall. Pet. Eng.*, **146**, 56–62.
- Bordes, C., Jouniaux, L., Dietrich, M., Pozzi, J.-P. & Garambois, S., 2006. First laboratory measurements of seismo-magnetic conversions in fluid-filled Fontainebleau sand, *Geophys. Res. Lett.*, **33**, L01302, doi:10.1029/2005GL021587.
- Bordes, C., Jouniaux, L., Garambois, S., Dietrich, M., Pozzi, J.-P. & Gaffet, S., 2008. Evidence of the theoretically predicted seismo-magnetic conversion, *Geophys. J. Int.*, **174**, 489–504.
- Brooks, R.J. & Corey, A.T., 1964. Hydraulic properties of porous media, *Hydrol. Pap.*, **3**, 318–333.
- Darnet, M., Marquis, G. & Sailhac, P., 2003, Estimating aquifer hydraulic properties from the inversion of surface streaming potential (sp) anomalies, *Geophys. Res. Lett.*, **30**, 1679, doi:10.1029/2003GL017631.
- Darnet, M., Marquis, G. & Sailhac, P., 2006. Hydraulic stimulation of geothermal reservoirs: fluid flow, electric potential and microseismicity relationships, *Geophys. J. Int.*, **166**, 438–444.
- Davis, J.A., James, R.O. & Leckie, J., 1978. Surface ionization and complexation at the oxide/water interface, *J. Colloid Interface Sci.*, **63**, 480–499.
- Doussan, C. & Ruy, S., 2009. Prediction of unsaturated soil hydraulic conductivity with electrical conductivity, *Water Resour. Res.*, **45**, W10408, doi:10.1029/2008WR007309.
- Doussan, C., Jouniaux, L. & Thony, J.-L., 2002. Variations of self-potential and unsaturated flow with time in sandy loam and clay loam soils, *J. Hydrol.*, **267**, 173–185.
- Dupuis, J.C., Butler, K.E. & Keping, A.W., 2007. Seismoelectric imaging of the vadose zone of a sand aquifer, *Geophysics*, **72**, A81–A85.
- Finizola, A., Sortino, F., Lenat, J.-F. & Valenza, M., 2002. Fluid circulation at Stromboli volcano (Aeolian Islands, Italy) from self potential and CO₂ surveys, *J. Volc. Geotherm. Res.*, **116**, 1–18.
- Finizola, A., Lenat, J.-F., Macedo, O., Ramos, D., Thouret, J.-C. & Sortino, F., 2004. Fluid circulation and structural discontinuities inside Misti volcano (Peru) inferred from self-potential measurements, *J. Volc. Geotherm. Res.*, **135**(4), 343–360.
- Gardner, W.R., 1958. Some steady state solutions of the unsaturated moisture flow equation with application to evaporation from a water table, *Soil Sci.*, **85**, 228–232.
- van Genuchten, M.T., 1980. A closed-form equation for predicting the hydraulic conductivity of unsaturated soil, *Soil Sci. Soc. Am. J.*, **44**, 892–898.
- Gibert, D. & Pessel, M., 2001. Identification of sources of potential fields with the continuous wavelet transform: application to self-potential profiles, *Geophys. Res. Lett.*, **28**, 1863–1866.
- Glover, P.W.J. & Walker, E., 2009. Grain-size to effective pore-size transformation derived from electrokinetic theory, *Geophysics*, **74**, E17–E29.
- Glover, P.W.J., Zadjali, I.I. & Frew, K.A., 2006. Permeability prediction from MICP and NMR data using an electrokinetic approach, *Geophysics*, **71**, F49–F60.
- Guichet, X., Jouniaux, L. & Pozzi, J.-P., 2003. Streaming potential of a sand column in partial saturation conditions, *J. geophys. Res.*, **108**(B3), 2141, doi:10.1029/2001JB001517.
- Guichet, X., Jouniaux, L. & Catel, N., 2006. Modification of streaming potential by precipitation of calcite in a sand-water system: laboratory measurements in the pH range from 4 to 12, *Geophys. J. Int.*, **166**, 445–460.
- Hayek, M., Lehmann, F. & Ackerer, P., 2008. Adaptive multi-scale parametrization for one-dimensional flow in unsaturated porous media, *Adv. Water Resour.*, **31**, 28–43.
- Henry, P., Jouniaux, L., Scream, E.J., Hunze, S. & Saffer, D.M., 2003. Anisotropy of electrical conductivity record of initial strain at the toe of the Nankai accretionary wedge, *J. geophys. Res.*, **108**, 2407, doi:10.1029/2002JB002287.
- Ishido, T. & Mizutani, H., 1981. Experimental and theoretical basis of electrokinetic phenomena in rock water systems and its applications to geophysics, *J. geophys. Res.*, **86**, 1763–1775.
- Jaafar, M.Z., Vinogradov, J. & Jackson, M.D., 2009. Measurement of streaming potential coupling coefficient in sandstones saturated with high salinity NaCl brine, *Geophys. Res. Lett.*, **36**, L21306, doi:10.1029/2009GL040549.
- Jackson, M.D., 2010. Multiphase electrokinetic coupling: insights into the impact of fluid and charge distribution at the pore scale from a bundle of capillary tubes model, *J. geophys. Res.*, **115**, B07206, doi:10.1029/2009JB007092.
- Jouniaux, L., Lallemand, S. & Pozzi, J., 1994. Changes in the permeability, streaming potential and resistivity of a claystone from the Nankai prism under stress, *Geophys. Res. Lett.*, **21**, 149–152.
- Jouniaux, L., Zamora, M. & Reuschlé, T., 2006. Electrical conductivity evolution of non-saturated carbonate rocks during deformation up to failure, *Geophys. J. Int.*, **167**, 1017–1026.
- Jouniaux, L., Maeneult, A., Naudet, V., Pessel, M. & Sailhac, P., 2009. Review of self-potential methods in hydrogeophysics, *C. R. Geoscience*, **341**, 928–936.

- Lehmann, F. & Ackerer, P., 1998. Comparison of iterative methods for improved solutions of the fluid flow equation in partially saturated porous media, *Transp. Porous Media*, **31**, 275–292.
- Linde, N., Jougnot, D., Revil, A., Matthai, S.K., Renard, D. & Doussan, C., 2007. Streaming current generation in two-phase flow conditions, *Geophys. Res. Lett.*, **34**, L03306, doi:10.1029/2006GL028878.
- Lorne, B., Perrier, F. & Avouac, J.-P., 1999. Streaming potential measurements. 1. Properties of the electrical double layer from crushed rock samples, *J. geophys. Res.*, **104**(B8), 17 857–17 877.
- Maineult, A., Bernabé, Y. & Ackerer, P., 2006a. Detection of advected, reacting redox fronts from self-potential measurements, *J. Contam. Hydrol.*, **86**, 32–52, doi:10.1016/j.jconhyd.2006.02.007.
- Maineult, A., Jouniaux, L. & Bernabé, Y., 2006b. Influence of the mineralogical composition on the self-potential response to advection of KCl concentration fronts through sand, *Geophys. Res. Lett.*, **33**, L24311, doi:10.1029/2006GL028048.
- Maineult, A., Strobach, E. & Renner, J., 2008. Self-potential signals induced by periodic pumping test, *J. geophys. Res.*, **113**, B01203, doi:10.1029/2007JB005193.
- Mauri, G., Williams-Jones, G. & Saracco, G., 2010. Depth determinations of shallow hydrothermal system by self-potential and multi-scale wavelet tomography, *J. Volc. Geotherm. Res.*, **191**, 233–244.
- Mualem, Y., 1976. A new model for predicting the hydraulic conductivity of unsaturated porous media, *Water Resour. Res.*, **12**, 513–522.
- Naudet, V., Revil, A., Bottero, J.-Y. & Bégassat, P., 2003. Relationship between self-potential (SP) signals and redox conditions in contaminated groundwater, *Geophys. Res. Lett.*, **30**(21), doi:10.1029/2003GL018096.
- Onizawa, S., Matsushima, N., Ishido, T., Hase, H., Takakura, S. & Nishi, Y., 2009. Self-potential distribution on active volcano controlled by three-dimensional resistivity structure in Izu-Oshima, Japan, *Geophys. J. Int.*, **178**, 1164–1181.
- Onsager, L., 1931. Reciprocal relations in irreversible processes: I, *Phys. Rev.*, **37**, 405–426, doi:10.1103/PhysRev.37.405.
- Overbeek, J.T.G., 1952. Electrochemistry of the double layer, in *Colloid Science, Irreversible Systems*, Vol. 1, pp. 115–193, ed. Kruyt, H.R., Elsevier, Amsterdam.
- Perrier, F. & Morat, P., 2000. Characterization of electrical daily variations induced by capillary flow in the non-saturated zone, *Pure appl. Geophys.*, **157**, 785–810.
- Pinder, G.F. & Gray, W.G., 1977. *Finite Element Simulation in Surface and Subsurface Hydrology*, Academic Press, New York, NY.
- Pozzi, J.-P. & Jouniaux, L., 1994. Electrical effects of fluid circulation in sediments and seismic prediction, *C.R. Acad. Sci. Paris, II*, **318**(1), 73–77.
- Press, W.H., Teukolsky, S., Vetterling, W.T. & Flannery, B.P., 1992. *Numerical Recipes in Fortran: The art of Scientific Computing*, 2nd edn, Cambridge University Press, Cambridge.
- Pride, S., 1994. Governing equations for the coupled electromagnetics and acoustics of porous media, *Phys. Rev. B*, **50**, 15 678–15 695.
- Pride, S. & Morgan, F.D., 1991. Electrokinetic dissipation induced by seismic waves, *Geophysics*, **56**(7), 914–925.
- Revil, A. & Linde, N., 2011. Comment on ‘Streaming potential dependence on water-content in Fontainebleau sand’ by V. Allègre, L. Jouniaux, F. Lehmann and P. Sailhac, *Geophys. J. Int.*, **186**, 113–114, doi:10.1111/j.1365-246X.2010.04850.x.
- Revil, A., Linde, N., Cerepi, A., Jougnot, D., Matthai, S. & Finsterle, S., 2007. Electrokinetic coupling in unsaturated porous media, *J. Colloid Interface Sci.*, **313**, 315–327.
- Richards, L.A., 1931. Capillary conduction of liquids through porous medium, *Physics*, **1**, 318–333.
- Sailhac, P., Darnet, M. & Marquis, G., 2004. Electrical streaming potential measured at the ground surface: forward modeling and inversion issues for monitoring infiltration and characterizing the vadose zone, *Vadose Zone J.*, **3**, 1200–1206.
- Saracco, G., Labazuy, P. & Moreau, F., 2004. Localization of self-potential sources in volcano-electric effect with complex continuous wavelet transform and electrical tomography methods for an active volcano, *Geophys. Res. Lett.*, **31**, L12610, doi:10.1029/2004GL019554.
- Saunders, J.H., Jackson, M.D. & Pain, C.C., 2008. Fluid flow monitoring in oilfields using downhole measurements of electrokinetic potential, *Geophysics*, **73**, E165–E180.
- Sheffer, M.R. & Oldenburg, D.W., 2007. Three-dimensional modelling of streaming potential, *Geophys. J. Int.*, **169**, 839–848.
- Thony, J.L., Morat, P., Vachaud, G. & Mouél, J.L., 1997. Field characterization of the relationship between electrical potential gradients and soil water flux, *C. R. Acad. Sci. Paris, Earth planet. Sci.*, **325**, 317–321.
- Tosha, T., Matsushima, N. & Ishido, T., 2003. Zeta potential measured for an intact granite sample at temperatures to 200°C, *Geophys. Res. Lett.*, **30**(6), doi:10.1029/2002GL016608.
- Vinogradov, J., Jaafar, M. & Jackson, M.D., 2010. Measurement of streaming potential coupling coefficient in sandstones saturated with natural and artificial brines at high salinity, *J. geophys. Res.*, **115**, B12204, doi:10.1029/2010JB007593.